

The Infrared Spectrum of Pyrene Anion in the CH Stretching Region

Heinrich Salzmann,^a Anne B. McCoy,^{b#} and J. Mathias Weber^{a}*

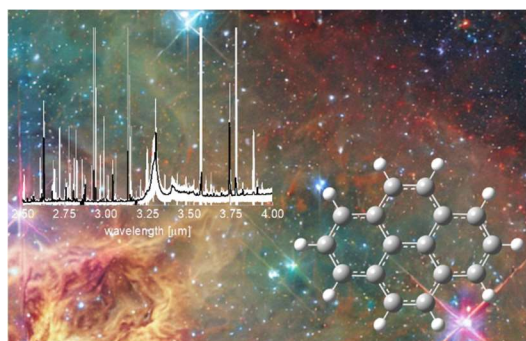
^aJILA and Department of Chemistry, University of Colorado, Boulder, CO 80309-0440, USA

^b Department of Chemistry, University of Washington, Seattle, WA 98195, USA

KEYWORDS.

Pyrene; polyaromatic hydrocarbons; astrochemistry; vibrational spectroscopy;

TOC Graphic



ABSTRACT

In this work, we report the infrared spectrum of pyrene anion, measured using messenger tagging with up to three Ar atoms. We assign the spectrum using density functional theory and vibrational perturbation theory. We discuss our results in the context of computed and experimental spectra from the literature as well as recent observations from astronomical sources, showing that PAH anions could contribute to the strong infrared emission bands at 3.29 μm from carbon rich regions of space.

Introduction

Polycyclic aromatic hydrocarbons (PAH) occur in many chemical contexts in nature as well as in technology. They are commonly found pollutants,¹⁻⁷ from various combustion processes,⁸ and are models for graphenic materials, such as carbon nanotubes and graphene.⁹⁻¹⁰ They are ubiquitous in astrochemistry, as they are present in astrochemical dust and ices,¹¹⁻¹⁸ and they have been widely investigated as emitters of diffuse interstellar bands (DIBs) and unidentified infrared emissions (UIEs).¹⁹⁻²⁹ A large body of work has been aimed at identifying PAHs in astrochemical environments and attribute their contributions to the DIBs and UIEs through experimental^{28, 30-49} and computational studies.^{26, 50-58} Computational data in current astrochemical databases⁵⁹⁻⁶¹ need to be validated through experimental data, particularly since improvements in observation, e.g., from the James Webb Space Telescope (JWST),²⁹ yield increased detail of spectroscopic information. Together with laboratory data, these developments will enable more accurate modeling of astrochemical processes.

Most previous gas-phase spectroscopy work focused primarily on cationic and neutral PAHs due to the assumed relative scarcity of anions in interstellar environments. However, despite their lower abundance, anions are relevant in astrochemistry and have been detected in space.⁶² In the absence of intense ultraviolet radiation in dense cold molecular clouds, anionic species potentially contribute uniquely to the astrochemical environment through electron attachment.^{51, 63-65} In addition, the CH stretching transitions in PAH cations are likely weak compared to neutral and anionic PAHs,^{37-38, 51, 53} lending additional importance to experimental data on anions. Similar to other PAHs with four rings, pyrene (Py) has a positive electron affinity (0.406 ± 0.010 eV⁶⁶) and can thereby form stable anions. While electronic transitions of Py⁻ are resonances in the

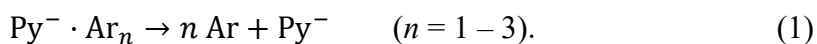
electron detachment continuum,⁶⁷ the CH stretching vibrational transitions in this class of PAHs are below the detachment limit and can therefore be expected to yield sharp vibrational bands.

Infrared spectra from carbon-rich astrochemical environments in the CH stretching region are congested and consist of contributions from many different species.^{19, 27, 51} Moreover, the CH stretching region of PAHs is challenging to interpret, due to Fermi resonances of the CH stretching fundamental transitions with overtones and combination bands of CH bending modes.^{26, 48-49, 52, 55-56, 58} In this work, we report the IR spectrum of gas-phase Py anions in the CH stretching region by IR messenger photodissociation spectroscopy using Ar atoms as messenger tags. We use anharmonic calculations to assign the dominant vibrational states in the spectrum.

Methods

Experimental. The photodissociation spectrometer used for this work has been described in detail in earlier work.⁶⁸⁻⁶⁹ Cluster ions of the form $\text{Py}^- \cdot \text{Ar}_n$ ($n = 1 - 3$) were generated by entrainment of Py vapor from an oven at $T = (400 \pm 10)$ K into a pulsed supersonic expansion of Ar (Even Lavié valve, stagnation pressure 1.5 bar), where fast electrons (800 eV) created an electron impact plasma. Target anion formation resulted from the attachment of slow secondary electrons to neutral precursors in the beam. Figure 1 shows a mass spectrum of the ion source under typical source conditions. Negative ions in the expansion plume were accelerated into a custom-built Wiley-McLaren time-of-flight spectrometer, where they were mass selected by an interleaving comb mass gate and subsequently irradiated with the output of a tunable OPO/OPA laser system (pulse duration: 5-7 ns, bandwidth: 2-5 cm^{-1} , pulse energy: 5-10 mJ) in a multipass cell. The wavelength of the light source was calibrated by gathering a photoacoustic spectrum of water⁷⁰ in a 3D-printed photoacoustic spectrometer tube, and we estimate the absolute error bars

of frequencies reported here to be $\pm 3 \text{ cm}^{-1}$. Upon photon absorption, the weakly bound argon atoms dissociate according to



Py^- fragment ions were separated from undissociated target ions in a two-stage reflectron, and their intensity was monitored on a dual microchannel plate detector. The fragment ion intensity was normalized to the photon fluence to generate IR photodissociation spectra. To ensure reproducibility and improve the signal to noise ratio, several spectra were taken on different days and averaged.

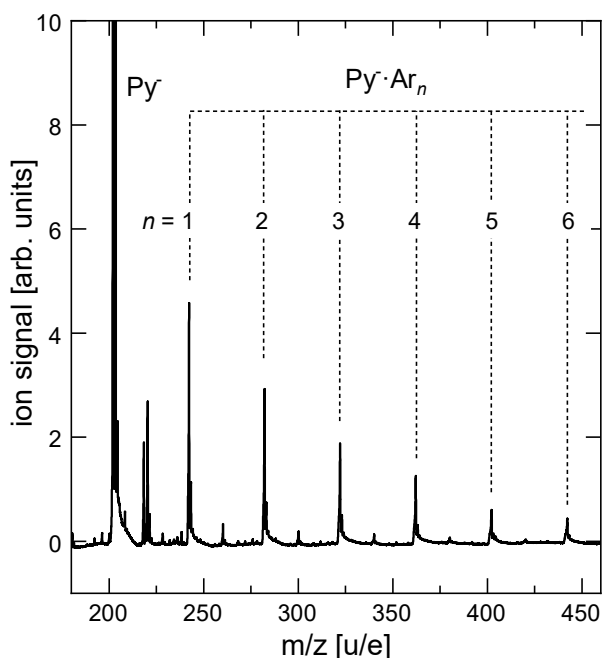


Figure 1. Reflectron time-of-flight mass spectrum under typical source conditions. The ion signal of the untagged Py^- ion is ca. 50 – 100 times greater than that of $\text{Py}^- \cdot \text{Ar}$. The weaker peaks between the $\text{Py}^- \cdot \text{Ar}_n$ progression are due to $\text{Py}^- \cdot \text{H}_2\text{O} \cdot \text{Ar}_n$ ions.

Computational. The structure of Py⁻ was optimized employing density functional theory (DFT) using the B3LYP⁷¹⁻⁷² functional and 6-311+G basis sets⁷³⁻⁷⁴ for all atoms. Harmonic calculations are insufficient to describe the CH stretching region of the IR spectrum of PAH molecules, since many of the CH stretching fundamental transitions are nearly degenerate with overtones and combination bands of CH bending modes, borrowing intensity through Fermi resonances and resulting in highly congested spectra.^{55, 58, 75-76} We therefore used second order vibrational perturbation theory (VPT2)⁷⁷⁻⁷⁸ calculations to assign the features in the experimental spectrum, employing the same functional and basis sets as for the structure optimization, consistent with the typical recommendation⁷⁷ that triple- ζ basis sets with polarizable (and in the present case also diffuse) functions is recommended for such calculations. To accelerate the calculations in a system the size of Py⁻ and to ensure that spectroscopic selection rules are obeyed, we enforced D_{2h} symmetry for some of the calculations, with the molecule in the yz plane. All calculations were carried out using Gaussian 16.⁷⁸ Note that we use Herzberg notation for the vibrational modes.

Analysis of the results of these calculations, showed some problematic trends. Specifically, some of the CH stretching fundamental transitions that should be forbidden by symmetry (here: a_g and b_{3g} modes under the D_{2h} point group symmetry) acquired significant intensities in the VPT2 calculations (see Supporting Information). Likewise, the VPT2 calculations predicted that some of the transitions that have two quanta of excitation in the same vibration (e. g. the $\nu = 2$ overtones), all of which should be forbidden by symmetry, acquired notable intensities when the symmetry was not strictly enforced. As described in the Supporting Information, we believe that the origin of the large intensities of symmetry forbidden transitions predicted by the VPT2 calculations most likely reflects numerical instabilities in the evaluation of the second derivatives of the potential. These derivatives are obtained through finite difference schemes where the fourth

derivatives are obtained by numerical evaluation of the elements of the Hessian in terms of the normal mode coordinates.⁷⁹⁻⁸¹ Analysis of the cubic and quartic contributions shows that there are a number of such terms, which couple states of different symmetries and have values that are approaching several cm^{-1} . While these terms will have a negligible effect on the energies, they will contribute to the second order correction to the wave functions, and through this, lead to the problematic intensities that are noted above (see Supporting Information). To address this issue, the transition moments used to obtain the anharmonic intensities were evaluated only through first order in perturbation theory. Operationally, this is equivalent to using the harmonic intensities for the $\Delta v = 1$ transitions and anharmonic intensities for $\Delta v = 2$ transitions. Because of the change in the transition moments used to calculate the spectra, we also reevaluated the intensities of transitions to any state involved in a Fermi resonance, replacing the deperturbed transition moments for the fundamental transitions with the corresponding harmonic values. A similar approach was taken in our recent study of host-guest complexes.⁸² To compare the harmonic and anharmonic calculated spectra with the experimental spectrum, we applied a scaling factor of 0.96 to the harmonic frequencies. All spectra were broadened by a Lorentzian line shape with 8 cm^{-1} full width at half maximum.

Results and Discussion

Figure 2.A shows the photodissociation spectrum of $\text{Py}^- \cdot \text{Ar}_2$ in the CH stretching region, monitoring the loss of both Ar atoms. We note that different levels of Ar solvation do not shift the observed features appreciably, as differences in the observed peak positions for $n = 1 - 3$ do not exceed 1 cm^{-1} (see Supporting Information). The near-absence of Ar-induced shifts strongly suggests that the spectrum shown in Figure 2 represents that of bare Py^- within our experimental

uncertainties. Out of the 72 vibrational modes of Py^- , 10 are CH stretching modes, and five of these are IR active, with b_{1u} or b_{2u} character. The experimental spectrum has several prominent features, all containing several unresolved or partially resolved transitions. Some of these features are qualitatively recovered by scaled harmonic calculations (Figure 2.C), specifically the peaks at 2982 cm^{-1} (labeled F_{24} in the experimental spectrum, F_{25} in the scaled harmonic calculation) and around 3021 cm^{-1} (F_{23} , F_{42}). The anharmonic treatment changes the frequencies and intensities of ω_{24} and ω_{25} significantly, and we ultimately assign the feature at 2982 cm^{-1} to the fundamental CH stretching transition belonging to the normal mode ω_{24} (see Figure 3 for mode pattern) rather than ω_{25} . The feature at 3021 cm^{-1} has a low-energy shoulder at 3014 cm^{-1} . Based on the calculated relative intensities, we assign the former to the fundamental transition of ω_{42} and the latter to that of ω_{23} .

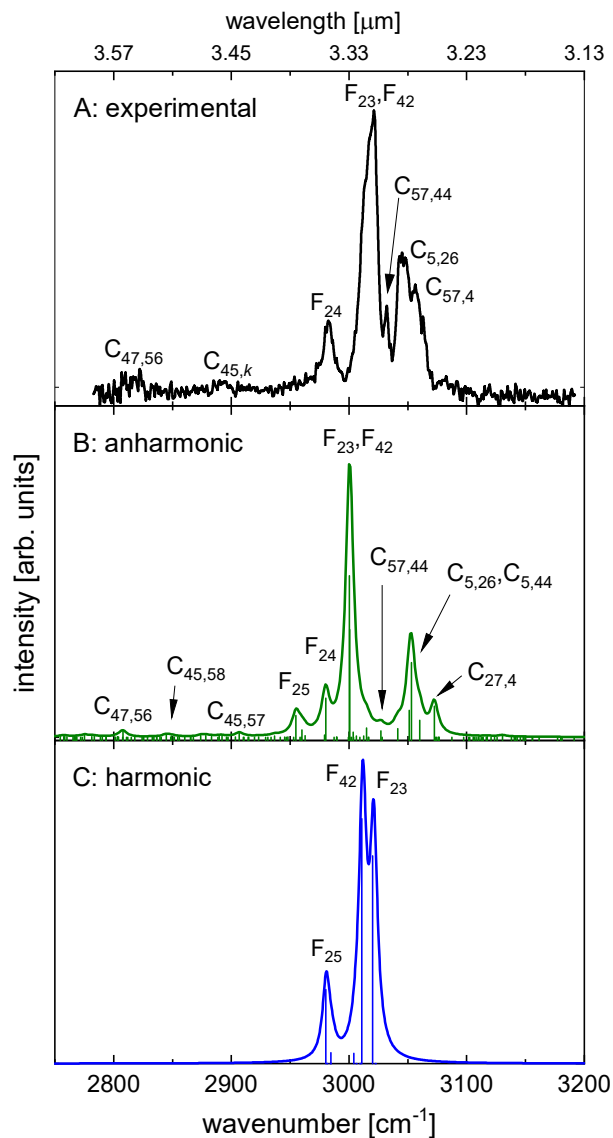


Figure 2. A: Experimental photodissociation spectrum of $\text{Py}^- \cdot \text{Ar}_2$. B: Anharmonic spectrum of Py^- with D_{2h} symmetry restriction. C: Harmonic approximation spectrum of Py^- with D_{2h} symmetry restriction. The labels describe the nature of the transitions: F_j = fundamental transition of mode j ; $C_{j,k}$ = combination band with $\Delta v = 1$ each in ω_j and ω_k . The assignment of the feature labeled $C_{45,k}$ in the experimental spectrum is ambiguous regarding the mode coupling to ω_{45} . The positions and intensities used for the calculated spectra are provided in the Supporting Information.

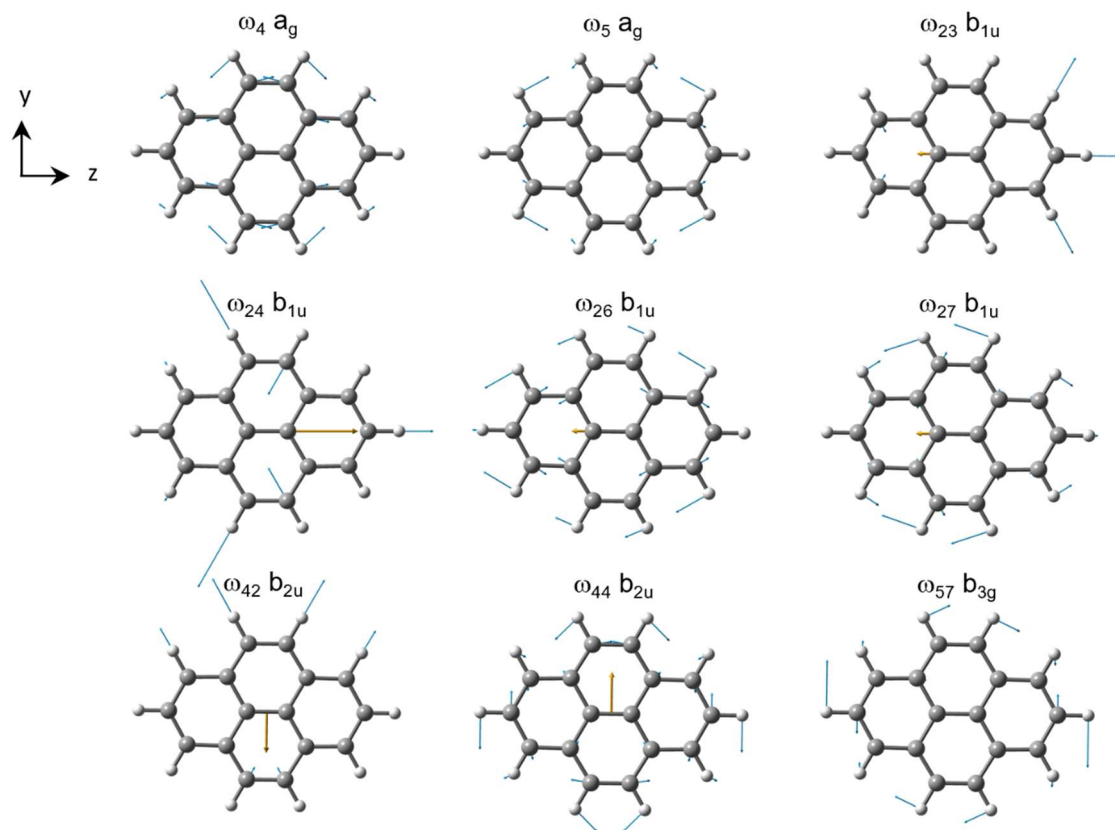


Figure 3. Vibrational normal modes (and their irreducible representations) with the most significant contributions to the IR spectrum of Py^- in the CH stretching region, either as fundamental transitions, or through Fermi interactions with CH stretching modes. Blue arrows show the normal mode pattern for each mode, while orange arrows represent dipole derivative vectors (where applicable).

None of the features at higher frequencies can be explained by harmonic calculations. Anharmonic calculations with D_{2h} symmetry restrictions (Figure 2.B) agree very well with the experimental spectrum. They show that these higher frequency features are due to combination bands of vibrational modes with in-plane CH bending and CC stretching character (see Figure 3 for mode patterns). We assign the narrow peak at 3032 cm^{-1} ($C_{57,44}$) to a combination band of ω_{57}

and ω_{44} . A peak at 3045 cm^{-1} ($C_{5,26}$, $C_{5,44}$) is due to combination bands of ω_5 with ω_{26} and ω_{44} , and a partially resolved shoulder at 3056 cm^{-1} ($C_{27,4}$) is due to a combination band of ω_{27} and ω_4 , or of ω_{56} and ω_{44} . At frequencies below the dominant group of peaks, we observe two broad, weak features and 2894 cm^{-1} and 2817 cm^{-1} , both of which are assigned to combination bands. All peaks and assignments are summarized in Table 1. We note that calculations without symmetry restriction recover the overall spectroscopic pattern with similar overall quality as the D_{2h} restricted calculations, but show some problematic intensity behavior as described in the Computational section.

Table 1. Assigned Transitions in the CH Stretching Spectrum of Py⁻

| observed [cm ⁻¹] | calculated ^a [cm ⁻¹] | assignment and symmetry ^b | calculated intensity (km/mol) |
|------------------------------|---|---|-------------------------------|
| 2817 ^d | 2808 | $\omega_{47}/\omega_{56}; b_{2u} \otimes b_{3g} = b_{1u}$ | 9.6 |
| 2893 ^c | 2845 ^d | $\omega_{58}/\omega_{45}; b_{3g} \otimes b_{2u} = b_{1u}$ | 3.6 |
| | 2907 ^d | $\omega_{45}/\omega_{57}; b_{2u} \otimes b_{3g} = b_{1u}$ | 5.7 |
| 2982 | 2980 (2985) | $\omega_{24} (b_{1u})$ | 59.0 |
| 3014 | 3000 ^e (3020) | $\omega_{23} (b_{1u})$ | 162.2 |
| 3021 | 3000 ^e (3011) | $\omega_{42} (b_{2u})$ | 243.8 |
| 3032 | 3027 | $\omega_{57}/\omega_{44}; b_{3g} \otimes b_{2u} = b_{1u}$ | 9.4 |
| 3045 | 3053 ^f | $\omega_5/\omega_{26}; a_g \otimes b_{1u} = b_{1u}$ | 112.5 |
| | 3051 ^f | $\omega_5/\omega_{44}; a_g \otimes b_{2u} = b_{2u}$ | 40.6 |
| 3056 | 3060 ^g | $\omega_{56}/\omega_{44}; b_{3g} \otimes b_{2u} = b_{1u}$ | 25.5 |
| | 3073 ^g | $\omega_{27}/\omega_4; b_{1u} \otimes a_g = b_{1u}$ | 47.0 |

^a anharmonic frequencies; for fundamental transitions, scaled harmonic frequencies are reported in parentheses;

^b entries with a single vibrational mode are fundamental transitions; entries with two different modes describe combination bands; the direct products result from the irreducible representations of each mode;

^c broad and weak;

^d either is a possible assignment for the feature at 2893 cm⁻¹;

^e the anharmonic frequency corrections for fundamental modes ω_{42} and ω_{23} resulted in the same frequency positions the assignment is based on their calculated relative intensities;

^f both likely contribute to the feature at 3045 cm⁻¹;

^g either is a possible assignment for the feature at 3056 cm⁻¹;

Figure 4 shows a comparison of IR data for neutral⁴⁷ and anionic Py in this range, together with the IR emission spectrum of M17, a star forming region in Sagittarius.²⁹ The CH stretching region of the IR spectrum of a PAH is strongly dependent on its charge state.^{51, 53} In PAH ions, the excess charge is delocalized throughout the π system.⁶⁶ In anions, excess electron density in the π system spills out into net antibonding orbitals of the CH groups, weakening the CH bonds and shifting the bulk of the CH stretching modes to lower frequencies compared to the neutral molecule,⁶⁸ which is observed for Py (Figure 4). In contrast, the cation bands are calculated to shift to higher frequencies compared to the neutral molecules, with the peak of the envelope of their bands 20-40 cm^{-1} higher than for the neutral molecules in most cases.^{51, 53}

The calculated IR intensities for Py^- are typically 3-10 times stronger than for neutral Py.^{51, 53} In contrast, the CH stretching modes in PAH cations are predicted to be very weak. While Saykally and coworkers³⁷⁻³⁸ reported experimental IR emission data on Py cations, their data in the CH stretching region are not sufficient to pinpoint individual transitions. Computational work on the different charge states of Py⁵³ predicts the intensities of the strongest CH stretching bands in Py cations to be ca. 10-200 times weaker than for neutral Py.^{51, 53}

Comparing the infrared photodissociation spectrum of $\text{Py}^- \cdot \text{Ar}_2$ with astronomical observations (Figure 4), and taking into account the average frequency positions and intensities calculated for anionic, neutral, and cationic PAHs,^{51, 53} it seems quite possible that the CH stretching features of PAH anions could contribute to the long-wavelength part of the prominent $3.29 \mu\text{m}$ (ca. 3040 cm^{-1}) feature, particularly in regions with low UV irradiation and high electron density.⁵¹

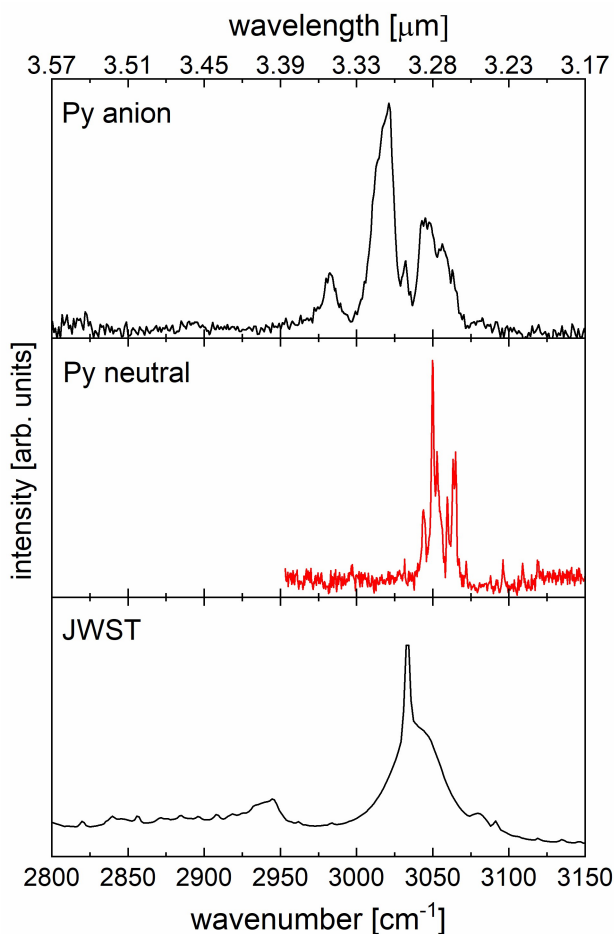


Figure 4. Comparison of experimental spectra of Py^- (top) and Py (center) with emission data of M17 (James Webb Space Telescope).²⁹ The data on neutral Py was taken from ref. ⁴⁷.

Conclusions

We report the IR spectrum of Py^- in the CH stretching region, measured using messenger tagging with Ar atoms, with the Ar induced shift of the bands less than 1 cm^{-1} . While the spectrum is dominated by several CH stretching fundamental bands, it cannot be satisfactorily interpreted with harmonic calculations. Anharmonic VPT2 calculations recover the experimental spectrum very well, with an average error of 11 cm^{-1} (0.36% and actual deviations from the experimental values between -9 cm^{-1} (-0.29%) and 21 cm^{-1} (0.70%), and they do not require the use of an empirical

scaling factor that needs to be applied to harmonic calculations. However, care must be taken to avoid problems with numerical instabilities in the evaluation of the second derivatives of the potential, which can lead to incorrect intensities. We assign several prominent bands to combination bands of in-plane CH bending vibrational modes, which gain intensity through Fermi resonances with CH stretching fundamentals. We show that messenger tagging of PAH radical anions provides an excellent approach to obtain experimental spectra for these species and to calibrate the quality of computations. Similar to the work by Mackie et al.⁵⁵ on neutral PAHs, our results show that VPT2 calculations can be used to significantly improve the predictions in computational databases.⁵⁹⁻⁶¹ Anharmonic calculations also will give better representations for the available states leading to possible IR emission upon electron attachment to Py and other PAHs.

ASSOCIATED CONTENT

Supporting Information. The following files are available free of charge.

SI_Vibrational_Analysis.xlsx (Excel file): Vibrational analysis.

SI_Salzmann_CH_stretches_in_Pyrene.pdf (PDF file): Dependence of the $\text{Py}^- \cdot \text{Ar}_n$ spectra on the number of Ar atoms, n ; atomic coordinates of Py^- ; Comments on Intensity Problems in Vibrational Perturbation Theory

AUTHOR INFORMATION

Corresponding Author

* J. Mathias Weber: weberjm@jila.colorado.edu

Anne B. McCoy: abmccoy@uw.edu

ACKNOWLEDGMENT

J. M. W. gratefully acknowledges support from the Department of Energy, Office of Basic Energy Sciences, under grant no. DE-SC0021387 and through the Physics Frontiers Center at JILA (PHY-2317149). A. B. M. gratefully acknowledges support from the National Science Foundation (CHE-2154126). We thank Prof. W. J. Buma (University of Amsterdam) for providing IR data on neutral Py and Dr. C. Boersma (NASA) for providing James Webb Space Telescope data.

REFERENCES

- (1) Han, Y. M.; Bandowe, B. A. M.; Schneider, T.; Pongpiachan, S.; Ho, S. S. H.; Wei, C.; Wang, Q. Y.; Xing, L.; Wilcke, W. A 150-Year Record of Black Carbon (Soot and Char) and Polycyclic Aromatic Compounds Deposition in Lake Phayao, North Thailand. *Env. Poll.* **2021**, *269*, 116148.
- (2) Li, X. R.; Zhao, Q.; Yang, Y.; Zhao, Z. Y.; Liu, Z. R.; Wen, T. X.; Hu, B.; Wang, Y. S.; Wang, L. L.; Wang, G. H. Composition and Sources of Brown Carbon Aerosols in Megacity Beijing During the Winter of 2016. *Atmos. Res.* **2021**, *262*, 105773.
- (3) Wang, J. F.; Ye, J. H.; Zhang, Q.; Zhao, J.; Wu, Y. Z.; Li, J. Y.; Liu, D. T.; Li, W. J.; Zhang, Y. G.; Wu, C.; et al. Aqueous Production of Secondary Organic Aerosol from Fossil-Fuel Emissions in Winter Beijing Haze. *Proc. Natl. Acad. Sci. U. S. A.* **2021**, *118*, e2022179118.
- (4) Mojiri, A.; Zhou, J. L.; Ohashi, A.; Ozaki, N.; Kindaichi, T. Comprehensive Review of Polycyclic Aromatic Hydrocarbons in Water Sources, Their Effects and Treatments. *Sci. Total Environ.* **2019**, *696*, 133971.
- (5) Bourotte, C.; Forti, M. C.; Taniguchi, S.; Bicego, M. C.; Lotufo, P. A. A Wintertime Study of PAHs in Fine and Coarse Aerosols in Sao Paulo City, Brazil. *Atmos. Env.* **2005**, *39*, 3799-3811.
- (6) Gogou, A.; Bouloubassi, I.; Stephanou, E. G. Marine Organic Geochemistry of the Eastern Mediterranean: 1. Aliphatic and Polyaromatic Hydrocarbons in Cretan Sea Surficial Sediments. *Marine Chem.* **2000**, *68*, 265-282.

(7) Yunker, M. B.; Macdonald, R. W.; Vingarzan, R.; Mitchell, R. H.; Goyette, D.; Sylvestre, S. PAHs in the Fraser River Basin: A Critical Appraisal of PAH Ratios as Indicators of PAH Source and Composition. *Org. Geochem.* **2002**, *33*, 489-515.

(8) Khalili, N. R.; Scheff, P. A.; Holsen, T. M. PAH Source Fingerprints for Coke Ovens, Diesel and Gasoline-Engines, Highway Tunnels, and Wood Combustion Emissions. *Atmos. Environ.* **1995**, *29*, 533-542.

(9) Chen, L.; Cooper, A. C.; Pez, G. P.; Cheng, H. Mechanistic Study on Hydrogen Spillover onto Graphitic Carbon Materials. *J. Phys. Chem. C* **2007**, *111*, 18995-19000.

(10) Berashevich, J.; Chakraborty, T. On the Nature of Interlayer Interactions in a System of Two Graphene Fragments. *J. Phys. Chem. C* **2011**, *115*, 24666-24673.

(11) Imanaka, H.; Khare, B. N.; Elsila, J. E.; Bakes, E. L. O.; McKay, C. P.; Cruikshank, D. P.; Sugita, S.; Matsui, T.; Zare, R. N. Laboratory Experiments of Titan Tholin Formed in Cold Plasma at Various Pressures: Implications for Nitrogen-Containing Polycyclic Aromatic Compounds in Titan Haze. *Icarus* **2004**, *168*, 344-366.

(12) Hardegree-Ullman, E. E.; Gudipati, M. S.; Boogert, A. C. A.; Lignell, H.; Allamandola, L. J.; Stapelfeldt, K. R.; Werner, M. Laboratory Determination of the Infrared Band Strengths of Pyrene Frozen in Water Ice: Implications for the Composition of Interstellar Ices. *Astrophys. J.* **2014**, *784*, 172.

(13) Quirico, E.; Moroz, L. V.; Schmitt, B.; Arnold, G.; Faure, M.; Beck, P.; Bonal, L.; Ciarniello, M.; Capaccioni, F.; Filacchione, G.; et al. Refractory and Semi-Volatile Organics at the

Surface of Comet 67p/Churyumov-Gerasimenko: Insights from the Virtis/Rosetta Imaging Spectrometer. *Icarus* **2016**, *272*, 32-47.

(14) Derenne, S.; Robert, F. Model of Molecular Structure of the Insoluble Organic Matter Isolated from Murchison Meteorite. *Meteorit. Planet. Sci.* **2010**, *45*, 1461-1475.

(15) Jenniskens, P.; Baratta, G. A.; Kouchi, A.; Degroot, M. S.; Greenberg, J. M.; Strazzulla, G. Carbon Dust Formation on Interstellar Grains. *Astron. Astrophys.* **1993**, *273*, 583-600.

(16) Tielens, A. Interstellar Polycyclic Aromatic Hydrocarbon Molecules. *Annu. Rev. Astron. Astrophys.* **2008**, *46*, 289-337.

(17) Bouwman, J.; Cuppen, H. M.; Bakker, A.; Allamandola, L. J.; Linnartz, H. Photochemistry of the PAH Pyrene in Water Ice: The Case for Ion-Mediated Solid-State Astrochemistry. *Astron. Astrophys.* **2010**, *511*.

(18) Tielens, A. G. G. M. *Molecular Astrophysics*. Cambridge University Press: Cambridge, 2021.

(19) Joblin, C.; Dhendecourt, L.; Leger, A.; Defourneau, D. Infrared-Spectroscopy of Gas-Phase PAH Molecules .1. Role of the Physical-Environment. *Astron. Astrophys.* **1994**, *281*, 923-936.

(20) Schlemmer, S.; Cook, D. J.; Harrison, J. A.; Wurfel, B.; Chapman, W.; Saykally, R. J. The Unidentified Interstellar Infrared Bands - PAHs as Carriers. *Science* **1994**, *265*, 1686-1689.

(21) da Cunha, E.; Charlot, S.; Elbaz, D. A Simple Model to Interpret the Ultraviolet, Optical and Infrared Emission from Galaxies. *Mon. Notices Royal Astron. Soc.* **2008**, *388*, 1595-1617.

(22) Ehrenfreund, P.; Charnley, S. B. Organic Molecules in the Interstellar Medium, Comets, and Meteorites: A Voyage from Dark Clouds to the Early Earth. *Annu. Rev. Astron. Astrophys.* **2000**, *38*, 427-483.

(23) Li, A. G.; Draine, B. T. Infrared Emission from Interstellar Dust. II. The Diffuse Interstellar Medium. *Astrophys. J.* **2001**, *554*, 778-802.

(24) Silva, L.; Granato, G. L.; Bressan, A.; Danese, L. Modeling the Effects of Dust on Galactic Spectral Energy Distributions from the Ultraviolet to the Millimeter Band. *Astrophys. J.* **1998**, *509*, 103-117.

(25) Weingartner, J. C.; Draine, B. T. Dust Grain-Size Distributions and Extinction in the Milky Way, Large Magellanic Cloud, and Small Magellanic Cloud. *Astrophys. J.* **2001**, *548*, 296-309.

(26) Barker, J. R.; Allamandola, L. J.; Tielens, A. G. G. M. Anharmonicity and the Interstellar Polycyclic Aromatic Hydrocarbon Infrared Emission Spectrum. *Astrophys. J.* **1987**, *315*, L61.

(27) Pech, C.; Joblin, C.; Boissel, P. The Profiles of the Aromatic Infrared Bands Explained with Molecular Carriers. *Astron. Astrophys.* **2002**, *388*, 639-651.

(28) Garkusha, I.; Fulara, J.; Sarre, P. J.; Maier, J. P. Electronic Absorption Spectra of Protonated Pyrene and Coronene in Neon Matrixes. *J. Phys. Chem. A* **2011**, *115*, 10972-10978.

(29) Boersma, C.; Allamandola, L. J.; Esposito, V. J.; Maragkoudakis, A.; Bregman, J. D.; Temi, P.; Lee, T. J.; Fortenberry, R. C.; Peeters, E. JWST: Deuterated PAHs, PAH Nitriles, and PAH Overtone and Combination Bands. I. Program Description and First Look. *Astrophys. J.* **2023**, *959*, 74.

- (30) Shan, J.; Suto, M.; Lee, L. C. 3.3 Micron Emission from Ultraviolet Excitation of Some Aromatic-Molecules. *Astrophys. J.* **1991**, *383*, 459-465.
- (31) Szczepanski, J.; Vala, M. Infrared Frequencies and Intensities for Astrophysically Important Polycyclic Aromatic Hydrocarbon Cations. *Astrophys. J.* **1993**, *414*, 646-655.
- (32) Vala, M.; Szczepanski, J.; Pauzat, F.; Parisel, O.; Talbi, D.; Ellinger, Y. Electronic and Vibrational-Spectra of Matrix-Isolated Pyrene Radical Cations - Theoretical and Experimental Aspects. *J. Phys. Chem.* **1994**, *98*, 9187-9196.
- (33) Zhang, K.; Guo, B.; Colarusso, P.; Bernath, P. F. Far-Infrared Emission Spectra of Selected Gas-Phase PAHs: Spectroscopic Fingerprints. *Science* **1996**, *274*, 582-583.
- (34) Hudgins, D. M.; Sandford, S. A. Infrared Spectroscopy of Matrix Isolated Polycyclic Aromatic Hydrocarbons. 1. PAHs Containing Two to Four Rings. *J. Phys. Chem. A* **1998**, *102*, 329-343.
- (35) Hudgins, D. M.; Sandford, S. A. Infrared Spectroscopy of Matrix Isolated Polycyclic Aromatic Hydrocarbons. 2. PAHs Containing Five or More Rings. *J. Phys. Chem. A* **1998**, *102*, 344-352.
- (36) Oomens, J.; van Roij, A. J. A.; Meijer, G.; von Helden, G. Gas-Phase Infrared Photodissociation Spectroscopy of Cationic Polyaromatic Hydrocarbons. *Astrophys. J.* **2000**, *542*, 404-410.
- (37) Kim, H. S.; Wagner, D. R.; Saykally, R. J. Single Photon Infrared Emission Spectroscopy of the Gas Phase Pyrene Cation: Support for a Polycyclic Aromatic Hydrocarbon Origin of the Unidentified Infrared Emission Bands. *Phys. Rev. Lett.* **2001**, *86*, 5691-5694.

- (38) Kim, H. S.; Saykally, R. J. Single-Photon Infrared Emission Spectroscopy of Gaseous Polycyclic Aromatic Hydrocarbon Cations: A Direct Test for Proposed Carriers of the Unidentified Infrared Emission Bands. *Astrophys. J., Suppl. Ser.* **2002**, *143*, 455-467.
- (39) Person, W. B.; Pimentel, G. C.; Schnepf, O. Infrared Studies of Naphthalene and Naphthalene-d8. *J. Chem. Phys.* **2004**, *23*, 230-233.
- (40) Biennier, L.; Salama, F.; Gupta, M.; O'Keefe, A. Multiplex Integrated Cavity Output Spectroscopy of Cold PAH Cations. *Chem. Phys. Lett.* **2004**, *387*, 287-294.
- (41) Huneycutt, A. J.; Casaes, R. N.; McCall, B. J.; Chung, C. Y.; Lee, Y. P.; Saykally, R. J. Infrared Cavity Ringdown Spectroscopy of Jet-Cooled Polycyclic Aromatic Hydrocarbons. *ChemPhysChem* **2004**, *5*, 321-326.
- (42) Bernstein, M. P.; Sandford, S. A.; Allamandola, L. J. The Mid-Infrared Absorption Spectra of Neutral Polycyclic Aromatic Hydrocarbons in Conditions Relevant to Dense Interstellar Clouds. *Astrophys. J., Suppl. Ser.* **2005**, *161*, 53-64.
- (43) Useli-Bacchitta, F.; Bonnamy, A.; Mulas, G.; Mallocci, G.; Toubanc, D.; Joblin, C. Visible Photodissociation Spectroscopy of PAH Cations and Derivatives in the Pirenea Experiment. *Chem. Phys.* **2010**, *371*, 16-23.
- (44) Brumfield, B. E.; Stewart, J. T.; McCall, B. J. Extending the Limits of Rotationally Resolved Absorption Spectroscopy: Pyrene. *J. Phys. Chem. Lett.* **2012**, *3*, 1985-1988.
- (45) Zack, L. N.; Maier, J. P. Laboratory Spectroscopy of Astrophysically Relevant Carbon Species. *Chem. Soc. Rev.* **2014**, *43*, 4602-4614.

(46) Bahou, M.; Wu, Y. J.; Lee, Y. P. Infrared Spectra of Protonated Coronene and Its Neutral Counterpart in Solid Parahydrogen: Implications for Unidentified Interstellar Infrared Emission Bands. *Angew. Chem. Int. Ed.* **2014**, *53*, 1021-1024.

(47) Maltseva, E.; Petrigani, A.; Candian, A.; Mackie, C. J.; Huang, X. C.; Lee, T. J.; Tielens, A.; Oomens, J.; Buma, W. J. High-Resolution IR Absorption Spectroscopy of Polycyclic Aromatic Hydrocarbons in the 3 μm Region: Role of Periphery. *Astrophys. J.* **2016**, *831*.

(48) Chakraborty, S.; Mulas, G.; Demyk, K.; Joblin, C. Experimental Approach to the Study of Anharmonicity in the Infrared Spectrum of Pyrene from 14 to 723 K. *J. Phys. Chem. A* **2019**, *123*, 4139-4148.

(49) Wiersma, S. D.; Candian, A.; Bakker, J. M.; Petrigani, A. Gas-Phase Spectroscopy of Photostable PAH Ions from the Mid- to Far-Infrared. *Mon. Notices Royal Astron. Soc.* **2022**, *516*, 5216-5226.

(50) Bauschlicher, C. W.; Langhoff, S. R.; Sandford, S. A.; Hudgins, D. M. Infrared Spectra of Perdeuterated Naphthalene, Phenanthrene, Chrysene, and Pyrene. *J. Phys. Chem. A* **1997**, *101*, 2414-2422.

(51) Bakes, E. L. O.; Tielens, A. G. G. M.; Bauschlicher, J. C. W.; Hudgins, D. M.; Allamandola, L. J. Theoretical Modeling of Infrared Emission from Neutral and Charged Polycyclic Aromatic Hydrocarbons. II. *Astrophys. J.* **2001**, *560*, 261.

(52) Cane, E.; Miani, A.; Trombetti, A. Anharmonic Force Fields of Naphthalene-H(8) and Naphthalene-D(8). *J. Phys. Chem. A* **2007**, *111*, 8218-8222.

(53) Naganathappa, M.; Chaudhari, A. Theoretical Infrared and Electronic Absorption Spectra of C₁₆H₁₀ Isomers, Their Ions and Doubly Ions. *Mon. Notices Royal Astron. Soc.* **2012**, *425*, 490-505.

(54) Saed, B.; Omidyan, R. Electronically Excited States of Protonated Aromatic Hydrocarbons: Phenanthrene and Pyrene. *J. Phys. Chem. A* **2013**, *117*, 2499-2507.

(55) Mackie, C. J.; Candian, A.; Huang, X. C.; Maltseva, E.; Petrignani, A.; Oomens, J.; Mattioda, A. L.; Buma, W. J.; Lee, T. J.; Tielens, A. The Anharmonic Quartic Force Field Infrared Spectra of Five Non-Linear Polycyclic Aromatic Hydrocarbons: Benz[a]anthracene, Chrysene, Phenanthrene, Pyrene, and Triphenylene. *J. Chem. Phys.* **2016**, *145*, 084313.

(56) Chen, T.; Mackie, C.; Candian, A.; Lee, T. J.; Tielens, A. Anharmonicity and the Infrared Emission Spectrum of Highly Excited Polycyclic Aromatic Hydrocarbons. *Astron. Astrophys.* **2018**, *618*.

(57) Dontot, L.; Spiegelman, F.; Zamith, S.; Rapacioli, M. Dependence Upon Charge of the Vibrational Spectra of Small Polycyclic Aromatic Hydrocarbon Clusters: The Example of Pyrene. *Eur. Phys. J. D* **2020**, *74*.

(58) Mackie, C. J.; Candian, A.; Lee, T. J.; Tielens, A. G. G. M. Anharmonicity and the Ir Emission Spectrum of Neutral Interstellar PAH Molecules. *J. Phys. Chem. A* **2022**, *126*, 3198-3209.

(59) Bauschlicher, C. W.; Ricca, A.; Boersma, C.; Allamandola, L. J. The Nasa Ames PAH IR Spectroscopic Database: Computational Version 3.00 with Updated Content and the Introduction of Multiple Scaling Factors. *Astrophys. J., Suppl. Ser.* **2018**, *234*, 32.

(60) Boersma, C.; Bauschlicher, C. W.; Ricca, A.; Mattioda, A. L.; Cami, J.; Peeters, E.; de Armas, F. S.; Saborido, G. P.; Hudgins, D. M.; Allamandola, L. J. The Nasa Ames PAH IR Spectroscopic Database Version 2.00: Updated Content, Web Site, and on(Off)Line Tools. *The Astrophys. J., Suppl. Ser.* **2014**, *211*, 8.

(61) Mattioda, A. L.; Hudgins, D. M.; Boersma, C.; Bauschlicher, C. W.; Ricca, A.; Cami, J.; Peeters, E.; de Armas, F. S.; Saborido, G. P.; Allamandola, L. J. The Nasa Ames PAH IR Spectroscopic Database: The Laboratory Spectra. *Astrophys. J., Suppl. Ser.* **2020**, *251*, 22.

(62) Millar, T. J.; Walsh, C.; Field, T. A. Negative Ions in Space. *Chem. Rev.* **2017**, *117*, 1765-1795.

(63) Carelli, F.; Grassi, T.; Gianturco, F. A. Electron Attachment Rates for PAH Anions in the Ism and Dark Molecular Clouds: Dependence on Their Chemical Properties. *Astron. Astrophys.* **2013**, *549*, A103.

(64) Demarais, N. J.; Yang, Z.; Martinez, O.; Wehres, N.; Snow, T. P.; Bierbaum, V. M. Gas-Phase Reactions of Polycyclic Aromatic Hydrocarbon Anions with Molecules of Interstellar Relevance. *Astrophys. J.* **2012**, *746*, 32.

(65) Yang, Z.; Cole, C. A.; Martinez, O.; Carpenter, M. Y.; Snow, T. P.; Bierbaum, V. M. Experimental and Theoretical Studies of Reactions between H Atoms and Nitrogen-Containing Carbanions. *Astrophys. J.* **2011**, *739*, 19.

(66) Ando, N.; Kokubo, S.; Mitsui, M.; Nakajima, A. Photoelectron Spectroscopy of Pyrene Cluster Anions, (Pyrene)_N⁻ (N=1–20). *Chem. Phys. Lett.* **2004**, *389*, 279-283.

- (67) Lietard, A.; Verlet, J. R. R. Effect of Microhydration on the Temporary Anion States of Pyrene. *J. Phys. Chem. Lett.* **2022**, *13*, 3529-3533.
- (68) Knurr, B. J.; Adams, C. L.; Weber, J. M. Infrared Spectroscopy of Hydrated Naphthalene Cluster Anions. *J. Chem. Phys.* **2012**, *137*, 104303.
- (69) LeMessurier, N.; Salzman, H.; Lerversee, R.; Weber, J. M.; Eaves, J. D. Water-Hydrocarbon Interactions in Anionic Pyrene Monohydrate. *submitted* **2024**.
- (70) Wallace, W. E., Infrared Spectra. In *NIST Chemistry WebBook, NIST Standard Reference Database Number 69*, National Institute of Standards and Technology: Gaithersburg, MD.
- (71) Becke, A. D. Density-Functional Exchange-Energy Approximation with Correct Asymptotic-Behavior. *Phys. Rev. A* **1988**, *38*, 3098-3100.
- (72) Becke, A. D. Density-Functional Thermochemistry .3. The Role of Exact Exchange. *J. Chem. Phys.* **1993**, *98*, 5648-5652.
- (73) McLean, A. D.; Chandler, G. S. Contracted Gaussian-Basis Sets for Molecular Calculations .1. 2nd Row Atoms, Z=11-18. *J. Chem. Phys.* **1980**, *72*, 5639-5648.
- (74) Krishnan, R.; Binkley, J. S.; Seeger, R.; Pople, J. A. Self-Consistent Molecular-Orbital Methods .20. Basis Set for Correlated Wave-Functions. *J. Chem. Phys.* **1980**, *72*, 650-654.
- (75) Sibert, E. L.; Kidwell, N. M.; Zwier, T. S. A First-Principles Model of Fermi Resonance in the Alkyl Ch Stretch Region: Application to Hydronaphthalenes, Indanes, and Cyclohexane. *J. Phys. Chem. B* **2014**, *118*, 8236-8245.

(76) Sibert, E. L.; Tabor, D. P.; Kidwell, N. M.; Dean, J. C.; Zwier, T. S. Fermi Resonance Effects in the Vibrational Spectroscopy of Methyl and Methoxy Groups. *J. Phys. Chem. A* **2014**, *118*, 11272-11281.

(77) Franke, P. R.; Stanton, J. F.; Douberly, G. E. How to Vpt2: Accurate and Intuitive Simulations of Ch Stretching Infrared Spectra Using VPT2+K with Large Effective Hamiltonian Resonance Treatments. *J. Phys. Chem. A* **2021**, *125*, 1301-1324.

(78) Frisch, M. J.; Trucks, G. W.; Schlegel, H. B.; Scuseria, G. E.; Robb, M. A.; Cheeseman, J. R.; Scalmani, G.; Barone, V.; Petersson, G. A.; Nakatsuji, H.; et al. *Gaussian 16 Rev. C.01*, Wallingford, CT, 2016.

(79) Schneider, W.; Thiel, W. Anharmonic Force Fields from Analytic Second Derivatives: Method and Application to Methyl Bromide. *Chem. Phys. Lett.* **1989**, *157*, 367-373.

(80) Yang, Q.; Mendolicchio, M.; Barone, V.; Bloino, J. Accuracy and Reliability in the Simulation of Vibrational Spectra: A Comprehensive Benchmark of Energies and Intensities Issuing from Generalized Vibrational Perturbation Theory to Second Order (GVPT2). *Front. Astron. Space Sci.* **2021**, *8*, 665232.

(81) McCoy, A. B.; Boyer, M. A. Exploring Expansions of the Potential and Dipole Surfaces Used for Vibrational Perturbation Theory. *J. Phys. Chem. A* **2022**, *126*, 7242-7249.

(82) Terry, L. M.; Foreman, M. M.; Rasmussen, A. P.; McCoy, A. B.; Weber, J. M. Probing Ion-Receptor Interactions in Halide Complexes of Octamethyl Calix[4]Pyrrole. *submitted 2024*, Preprint at <https://doi.org/10.26434/chemrxiv-2023-59dcd>

TOC Graphic

